This is a preprint, the final version is subject to change, of the American Mineralogist (MSA)
Cite as Authors (Year) Title. American Mineralogist, in press.
(DOI will not work until issue is live.) DOI: http://dx.doi.org/10.2138/am-2016-5477

REVISION 1

"Satellite monazites" in polymetamorphic basement rocks of the Alps: their origin and petrological significance

FRITZ FINGER[1], ERWIN KRENN[1], BERNHARD SCHULZ[2], DANIEL HARLOV[3,4], DAVID SCHILLER[1]

[1] Department of Materials Engineering and Physics, University of Salzburg, Hellbrunnerstraße 34, 5020 Salzburg, Austria (e-mail: Friedrich.Finger@sbg.ac.at)

[2] Department of Economic Geology and Petrology, Institute of Mineralogy, TU Bergakademie Freiberg, Brennhausgasse 14, D-09596 Freiberg/Saxony, Germany

[3] GeoForschungsZentrum Potsdam, Telegrafenberg, D-14473 Potsdam, Germany

[4] Department of Geology, University of Johannesburg P.O. Box 524, Auckland Park, 2006 South Africa

ABSTRACT

Allanite-fluorapatite reaction coronas around monazite are abundant in metamorphic rocks. We report here special cases where a new generation of "satellite" monazite grains formed within these coronas. Using examples from different *P-T* regions in the eastern Alps, we examine the origin and the petrological significance of this complex mineralogical association by means of the electron microprobe utilizing Th-U-Pb monazite dating and high resolution BSE imaging. Satellite monazite grains form when a monazite bearing rock is metamorphosed in the allanite stability field (partial breakdown of first generation monazite to fluorapatite plus allanite), and is then heated to temperatures that permit a back reaction of fluorapatite + allanite to secondary satellite monazite grains surrounding the remaining original first generation monazite. Depending on the whole rock geochemistry satellite monazites can form under upper greenschist- as well as

amphibolite-facies conditions. In each of the three examples focused on here, the inherited core monazite was resistant to recrystallization and isotopic resetting, even though in one of the samples the metamorphic temperatures reached 720 °C. This shows that in greenschist- and amphibolite-facies polymetamorphic rocks, individual grains of inherited and newly formed monazite can and often will occur side by side. The original, inherited monazite will preferentially be preserved in low-Ca, high-Al lithologies, where its breakdown to allanite plus fluorapatite is suppressed. Conversely, a medium or high-Ca, monazite-bearing rock will become particularly fertile for secondary monazite regrowth after passing through a phase of strong retrogression in the allanite stability field. Based on this knowledge, specific sampling strategies for monazite dating campaigns in polymetamorphic basement can be developed.

Key words: Monazite, fluorapatite, allanite, metamorphic rocks, geochronology

INTRODUCTION

Monazite ($LREEPO_4$) and allanite ($CaREEAl_2FeSi_3O_{11}O(OH)$) are widespread accessory minerals in metamorphic rocks and one of the major hosts for the light rare earth elements (LREE) (Spear and Pyle 2002, Gieré and Sorensen 2004). Both minerals are of importance for U-Th-Pb geochronology as well (Parrish 1990, Harrison et al. 2002, Romer and Siegesmund 2003).

In general, monazite and allanite are not stable together. This was recognized already in very early accessory mineral studies (Lee and Dodge 1964, Lee and Bastron 1967). Monazite can react to allanite plus fluorapatite and vice versa (Finger et al. 1998, Wing et al. 2003). Whether monazite or allanite occurs in a metamorphic rock is determined by whole rock composition and the metamorphic grade (Janots et al. 2007, 2008, Spear 2010). For average metapelites there is a rule that allanite is stable under upper greenschist-facies conditions, and monazite under

amphibolite facies conditions (Smith and Barreiro 1990, Wing et al. 2003, Goswami-Benerjee and Robyr 2015). However, a higher CaO whole rock content expands the allanite stability field to higher temperatures and the monazite stability field then retreats to granulite facies conditions (Bingen et al. 1996). On the other hand, in rocks with a low CaO content, monazite may be stable at T < 500°C (Spear 2010). Also, a high whole rock Al content exerts an influence on the allanite-monazite transition, stabilizing monazite to lower temperatures (Spear 2010). The alteration of monazite to allanite and fluorapatite has been experimentally studied by Budzyn et al. (2011). Their work confirms the strong influence of fluid and whole rock composition on the stability of monazite. Both, monazite and allanite can occasionally alter to REE carbonate minerals like hydroxylbastnäsite-(Ce) or synchysite, when CO_2 rich fluids are present (Ondrejka et al. 2012, Hirtopanu et al. 2013).

An often observed metamorphic reaction texture in nature is the replacement of monazite by fluorapatite-allanite coronas (Finger et al. 1998, Broska and Siman 1998, Grapes et al. 2005, Majka and Budzyn 2006, Upadhyay and Pruseth 2012). This texture is mostly seen in metagranites with magmatic monazite that became metamorphosed under low- to medium T conditions. However, it can also occur in metapelites, if the monazite first formed during a higher-T metamorphic event and then reacted to fluorapatite plus allanite during a second lower-T metamorphic overprint (e.g. Bankhammer 2004, Gasser et al. 2012).

Puzzling cases have been reported from polymetamorphic rocks of the eastern Alps, where small monazite grains straddle such metamorphic fluorapatite-allanite coronas. This phenomenon has been termed satellite monazites (Krenn and Finger 2006), because the small monazite grains are arranged like satellites concentrically around a core monazite. The hypothesis was put forward that the satellite monazites formed through a back-reaction between fluorapatite and allanite (Krenn and Finger 2006), thus constituting an important textural indicator for polymetamorphic

rock evolution. Alternatively, one could argue that the "satellites" may perhaps just be the undigested remains from the periphery of the primary monazite.

In order to reveal the origin of this peculiar microstructural phenomenon we have carried out a detailed electron microprobe (EMP) study on three selected examples of polymetamorphic rocks from the eastern Alps. Apart from careful phase identification under high-resolution back scattered electron (BSE) imaging, the monazite Th-U-Pb dating method was applied utilizing the EMP data (Suzuki et al. 1991, Montel et al. 1996). These three case studies permit the problem of allanite-monazite stability in metamorphic rocks to be viewed from a new angle and also provide useful information with regard to the application and the potential of monazite geochronology in polymetamorphic terrains.

SAMPLE MATERIALS

The first sample is a mica schist from the polymetamorphic Zwölferzug formation in the northern Tauern Window (Fig. 1). This formation represents a Proterozoic to Paleozoic volcano-sedimentary sequence (Frank et al. 1987). It was first metamorphosed at amphibolite-facies conditions during the Variscan orogeny (i.e., in the Carboniferous) and then for a second time at upper greenschist-facies conditions during Alpine nappe stacking in the Tertiary (Von Quadt 1992). Peak *P-T* estimates for the Variscan metamorphic event are ~ 8 kbar and ~ 650 °C (Bankhammer 2004). *P-T* estimates for Tertiary (Alpine) regional metamorphism in this area are 3 – 5 kbar and 400 – 450 C° and define the apex of a clockwise *P-T* path (Dachs et al. 1991). The investigated thin section consists of ~50 % albite (including some 0.5 – 2 cm large albite porphyroblasts), ~30 % quartz, ~15 % muscovite, ~5 % chlorite (sometimes in mm-sized pseudomorphs after garnet) and a few small grains of epidote. In terms of geochemistry, the rock

is a low-Ca metapelite (Shaw 1956) with a CaO content of ~ 0.9 wt. % and an Al_2O_3 content of ~ 17 wt. %.

The second sample is a kyanite-garnet-mica schist from the Preims formation of the Saualpe Crystalline Unit (Weissenbach and Pistotnik 2000), which is part of the Middle Austro-alpine nappe system (Fig. 1). The Saualpe crystalline unit experienced prominent high-grade Permian regional metamorphism at low to medium pressures (Schuster and Stüwe 2008) and another phase of high-pressure amphibolite- to eclogite facies metamorphism in the Cretaceous, during the Alpine orogeny (Thöni and Miller 1996). Geothermobarometric investigations in the Preims unit (Schulz 2013) indicate peak conditions of ~750 °C/ 6 kbar for the Permian event and ~720 °C/14-16 kbar for the Cretaceous event. The studied sample consists approximately of 20 % garnet, 20 % quartz and plagioclase, 45 % biotite and muscovite, and about 15 % kyanite. The thin section contains a few large garnet porphyroblasts up to 5 mm in diameter with inclusions of mica, plagioclase, and quartz. Many small Alpine garnets with a grossular content higher than the Permian garnet are distributed in the foliation planes between the biotite and the muscovite. Lenticular, up to 10 mm sized aggregates of small kyanite crystals are aligned along the foliation. The CaO and Al_2O_3 whole rock contents are ~1.9 and ~19 wt.%, respectively, and thus close to the average metapelite of Shaw (1956).

The third sample is an orthogneiss from the Ötztal crystalline basement (Fig. 1). It is a medium- to coarse-grained, peraluminous S-type granite gneiss from the Sulztal metagranite unit (Schindlmayr 1999). The rock belongs to the Early Palaeozoic (Cambro-Ordovician) plutonic complex of the Ötztal crystalline basement (Hoinkes et al. 1997; Schindlmayr 1999). It was metamorphosed under amphibolite-facies conditions during the Variscan orogeny (550–650 °C, 4-7 kbar) and once more under upper greenschist-facies conditions (430-490 °C, 8-9 kbar) in the Cretaceous, during the Alpine orogeny (Tropper and Rechais 2003, Rode et al. 2012). The modal

content of sample 3 is ~30 % quartz, ~30 % plagioclase, ~30 % K-feldspar, muscovite, biotite, and chlorite. CaO and Al_2O_3 whole rock contents are ~1.8 and ~15 wt.%, respectively.

MONAZITE-FLUORAPATITE-ALLANITE MICROSTRUCTURES

Backscattered electron imaging (BSE), and phase identification with an energy-dispersive system (EDS), were carried out on a SEM Zeiss Ultraplus at Salzburg university and on a SEM FEI Quanta 600 FEG-MLA at the TU Bergakademie Freiberg.

Sample 1: Figure 2a shows a representative monazite from sample 1 that exhibits a fluorapatite-allanite-epidote corona with numerous small satellite monazites. The ~ 70 μm large, central monazite grain (termed as M1) is surrounded by a narrow 5 – 20 μm wide fluorapatite shell (dark in the image) and a 20-50 μm broad mantle of mainly allanite and epidote. The boundary between the fluorapatite shell and the allanite/epidote mantle is often irregularly shaped with spike-like protrusions, fringes, and indentations being present. Compared to epidote, the allanite appears a little brighter in the BSE image. Epidote can be found preferentially along the outer margin of the corona. Minor quartz, plagioclase, muscovite, and biotite were identified as well within and adjacent to the corona. The very bright, ~3-5 μm grains within the corona are for their most part monazite (termed as M2 in Fig. 2a). A few of them are xenotime. The M2 satellite monazites are, in general, positioned between fluorapatite and allanite and they have anhedral shapes. Minute bright grains within the fluorapatite ring are not monazite but most probably thorite or huttonite, judging from their high Th and Si signals in EDS. A precise analysis of these inclusions was not possible due to the small grain size.

Sample 2: The reaction textures are slightly different in this sample from the Saualpe Crystalline Unit. Only a small amount of allanite is preserved here. Central, ~ 30-80 μm large M1 monazite grains are surrounded by a fluorapatite ring and by numerous smaller satellite M2 monazite crystals. A representative example is shown in Fig. 2b. Muscovite, some biotite, and some kyanite occur in the neighbourhood of the satellite monazites together with quartz. The core M1 monazite often has a weak zonation showing a discrete, thin rim zone that is slightly brighter in the BSE image (Fig. 2b). Xenotime is not observed.

Sample 3: Figure 2c shows a representative satellite monazite structure from the Ötztal orthogneiss sample. The central M1 monazite grains are commonly very small and surrounded by large fluorapatite zones. Larger central M1 monazite grains (~30–40 μm) are rare and have been observed only three times in the thin section. There were also several cases, where no M1 monazite was visible and fluorapatite occupied the centre. The fluorapatite is surrounded by a fine-scale composite mineral mix of allanite and epidote with some inclusions of quartz, plagioclase, muscovite and biotite. Within this composite, satellite M2 monazites occur as up to 30 μm size grains. They often show finely serrated grain boundaries. In addition, the satellite monazite crystals are partly surrounded by narrow fluorapatite and allanite rings, a feature which has only been observed in sample 3. Xenotime appears to be absent.

ELECTRON MICROPROBE (EMP) TH-U-PB DATING OF MONAZITE

Monazite EMP analyses were performed on a JEOL JX 8600 electron microprobe at the University of Salzburg (samples 1 and 3) and on a JEOL JXA 8200 at the Geozentrum Nordbayern, University Erlangen (sample 2). Slightly different analysis routines are established in the two laboratories for Th-U-Pb monazite dating. The analytical parameters were as follows

(first value valid for Salzburg, second value in brackets valid for Erlangen): acceleration voltage 15 (20) kV, beam current 200 (100) nA, spot size 1-2 μm, 40 (30) seconds counting time for Pb on peak and 2 x 20 (10) seconds on background. This results in a statistical analytical error of typically 0.01 wt.% (1σ) for Pb.

The EMP analytical setup for monazite dating in both Salzburg and Erlangen follows the recommendations of Pyle et al. (2002) and Jercinovic and Williams (2005) with reference to the optimal choice of spectral lines, as well as background and line overlap corrections. More details, regarding calibration standards etc., can be found in Krenn et al. (2008) and Schulz and Schüssler (2013). The comparability of the dating results of both laboratories was controlled by measurements of the monazite standard Madmon (Schulz and Schüssler 2013).

Based on the measured concentrations of Th, U, and Pb, a chemical age was calculated for each monazite analysis using the equation of Montel et al. (1996). In addition, based on the EMP analytical uncertainties and following the procedure of Montel et al. (1996), an individual 2-sigma error was always attributed to this age, which was mostly between 50 and 70 Ma. In order to better constrain a monazite forming event, weighted average ages (90 % c.l.) were retrieved from a larger number of analyses.

The geochronological results are graphically presented in Th* vs. total Pb isochron diagrams after Suzuki et al. (1991). Isochron ages (CHIME ages in terms of Suzuki et al. 1991) were calculated after the least-square method. It should be noted that the two slightly different methods for dating a monazite population (weighted average age vs. CHIME age) generally provided sufficiently consistent results during this study. This suggests that the dates are geologically meaningful and not significantly disturbed by common Pb or Pb loss.

Sample 1: Two large M1 monazite and thirteen satellite M2 monazite grains were analysed using EMP. M1 monazite was analysed at the core and at various rim positions. The obtained ages range from 326 (± 67) to 387 (± 64) Ma with a weighted mean of 363 ± 11 Ma (MSWD: 1.6) and an isochron date of 366 ± 52 Ma (isochron slope: 0.0164 ± 0.0023, Y-axis intersection: - 0.0014 ± 0.0003; MSWD value: 0.97, Fig. 3a).

EMP analyses of M2 monazite grains yielded very low Pb contents. Therefore, the calculation of single point Th-U-total Pb ages was difficult and not always possible. Longer counting times of up to 640 s were used for Pb, resulting in a detection limit as low as ~0.005 wt. %, but Pb contents sometimes remained below that. Th-U-total Pb dates from the M2 monazite grains with Pb contents greater than the detection limit range from 20 to 90 Ma and arrange themselves along a flat trend in the Th* vs. Pb isochron diagram (Fig. 3a).

Sample 2: Th-U-Pb dates obtained from EMP analyses of the M1 monazite cores cluster around a weighted mean age of 262 ± 11 Ma (MSWD 0.11, n=49) indicating formation of M1 monazite during the Permian regional metamorphic stage. The age of 262 ± 11 Ma is in excellent agreement with a garnet isochron of 263.5 ± 6.8 Ma published by Thöni (2003) for another garnet mica-schist from the Saualpe crystalline unit. The CHIME age for M1 monazite in sample 2 is 250 ± 34 Ma (isochron slope: 0.0111 ± 0.0015, Y-axis intersection: 0.0030 ± 0.0004; MSWD value 0.97, Fig. 3b).

Age dates for the satellite M2 monazite grains (21 analyses) are consistently younger and can be combined to give a weighted mean average age of 94 ± 14 Ma (MSWD 0.091, n=21). This age fits well with other age determinations for the Cretaceous metamorphic event in that area, such as a Sm-Nd garnet age of around 90 Ma published by Thöni (2003). The CHIME age for M2

monazite in sample 2 is 85 ± 34 Ma (isochron slope: 0.0038 ± 0.0015, Y-axis intersection: 0.0011 ± 0.0004; MSWD value: 0.97, Fig. 3b).

The thin rim zone that mantles the core M1 monazite yields a Cretaceous age (black symbols in Fig. 3b), similar to the accompanying satellite M2 monazite crystals.

Sample 3: In sample 3, 14 EMP analyses were carried out on three of the larger M1 monazite grains and 13 EMP analyses on the satellite M2 monazite grains. M1 monazite grains were analysed both in the core and at various rim positions. EMP Th-U-total Pb dates obtained for these M1 monazite grains range from 441 (± 61) to 512 (± 70) Ma with an average mean of 478 ± 11 Ma (MSWD: 1.6) and an isochron age of 455 ± 56 Ma (Fig. 3b). The corresponding Th* vs. Pb isochron has a slope of 0.0204 ± 0.0025, a Y-axis intersection value of 0.0058 ± 0.0004, and a MSWD value of 1.08 (Fig. 3b). The age obtained for the M1 monazite matches the time period in which the prominent Cambro-Ordovician plutonic event in the Ötztal Crystalline Unit took place (Hoinkes et al. 1997).

EMP analyses of satellite M2 monazites from sample 3 provide Variscan ages ranging from 301 (± 68) to 390 (± 75) Ma. They define a weighted mean date of 343 ± 15 Ma (MSWD: 1.9) and an isochron date of 338 ± 40 Ma (isochron slope: 0.0149 ± 0.0018, Y-axis intersection: 0.0021 ± 0.0003, MSWD: 1.4; Fig. 3b).

MONAZITE COMPOSITIONS

Natural monazite shows considerable chemical variability with regard to La/Nd ratios, Th/U ratios, or Y and HREE contents as well as with regard to the huttonite and cheralite coupled substitutions (Spear and Pyle 2002). Therefore, different genetic types of monazite are often characterized by different compositions. In particular, the Y (HREE) contents are useful

237 petrological markers, because they are a function of temperature (Heinrich et al. 1996, Pyle et al.
238 2001). Representative monazite EMP analyses from our study are given in Table 1.
239
240 **Sample 1:** The composition of the M1 monazite cores is characterized by 3 to 5 wt. % ThO_2; 0.7
241 to 1.4 wt. % UO_2, and very low Y_2O_3 < 0.1 wt.% (Fig. 4a). M2 monazite grains from sample 1
242 show 1-9 wt. % ThO_2 as well as lower U contents (< 0.7 wt.% UO_2) and higher Y contents (0.5-
243 1.2 wt.% Y_2O_3) compared to the M1 monazite. M1 and M2 monazite can clearly be discriminated
244 in a UO_2 vs. Y_2O_3 diagram (Fig. 4a).
245
246 **Sample 2:** Both monazite generations have similar ranges in ThO_2 (3-7 wt. %) and UO_2 (mostly
247 0.6-0.9 wt. %). The main difference is in the Y_2O_3 values, which lie between 1.4 and 2.2 wt. % in
248 M1 monazite and are significantly lower (< 0.4 wt. %) in the M2 monazite grains. As in sample
249 1, a clear chemical distinction is possible between the M1 and M2 monazite in a UO_2 vs. Y_2O_3
250 diagram (Fig. 4b). The small rim zone around the core M1 monazite (Fig. 2b) corresponds in
251 composition to the satellite M2 monazite grains and has a low Y content (black symbols in Fig.
252 4b).
253
254 **Sample 3:** M1 monazite grains yield 5-7 wt. % ThO_2, 0.2-1 wt. % UO_2, and 1.5-4 wt. % Y_2O_3.
255 M2 monazite grains have 2-6 wt. % ThO_2, 0.1-0.7 wt. % UO_2 and 0.8-3 wt. % Y_2O_3 (Fig. 4b). In
256 the case of sample 3, a clear chemical distinction between the M1 and M2 monazite grains is not
257 obtained (Fig. 4c).
258
259
260

DISCUSSION AND CONCLUSIONS

Satellite monazites – a typical phenomenon of polymetamorphic monazite growth

The appearance of satellite M2 monazite crystals in fluorapatite-allanite reaction coronas around M1 monazite can be interpreted in terms of a new metamorphic stage of monazite growth. Based on three examples from three different geological units of the Eastern Alps, it can be shown, by means of chemical Th-U-Pb dating, that satellite M2 monazites are always significantly younger than the M1 monazite cores.

In sample 1 (metapelite, Tauern Window) the M1 monazite grains are ~ 360 Ma old. They grew during amphibolite facies Variscan regional metamorphism. The Variscan event has also been recorded by other methods in other rocks of that area (Von Quadt 1992). The low Y contents in the M1 monazite (Fig. 4a, Tab. 1) indicate growth in the presence of garnet (Pyle et al. 2001, Foster et al. 2002).

Statistically, the age dates for the small satellite M2 monazites in sample 1 are not precise, because the Pb contents are generally very low. However, the fact that the Pb contents show little increase with respect to Th* and remain low in Th enriched monazite (Fig. 3a), leaves little doubt that they formed during upper greenschist-facies Alpine regional metamorphism, which occurred in the Tertiary (around 30 Ma). Variscan garnet was consumed during this event to form chlorite pseudomorphs thereby liberating Y. Therefore, the satellite M2 monazites could acquire higher Y contents compared to the M1 monazite grains. Even a little xenotime crystallized out together with the M2 monazite. The maximum Y_2O_3 values of ~ 1.1 wt. % measured in the M2 monazite grains are compatible with upper greenschist-facies temperatures of around 450 to 500 °C, if the geothermometers of Heinrich et al. (1997) and Pyle et al. (2002) are used as reference.

In sample 2 (metapelite, Saualpe crystalline unit), the older M1 monazite formed, according to its Th-U-Pb dates, during a prominent Permian rifting event, which is widely recorded in the area (Schuster and Stüwe 2008). However, it is not clear if the bulk of the monazite crystallized close to the Permian *P-T* peak (750°C, 6 kbar) or slightly before at lower T on the prograde path. Due to a lack of excess YPO_4 and, subsequently, free xenotime, the measured Y contents in monazite provide no reliable thermometric information and can only be used to infer a minimum crystallization temperature of 550-600 °C. Judging from the Al and Ca content of the host rock, the allanite to monazite transition should occur around 550 °C (Pyle 2010), rendering monazite formation at ~550-600 °C theoretically feasible. Nevertheless, we consider it equally possible that much of the Permian monazite actually precipitated close to the *P-T* peak from an (YPO_4 undersaturated) anatectic melt, because muscovite dehydration melting may have taken place at the given *P-T* conditions. Distinguishing between these two possibilities is not easy, because the Permian crystallization relations (inclusion relationships) between the monazite and other minerals, that would be most informative in such cases (Goswami-Banerjee and Robyr 2015), were widely destroyed during the Cretaceous metamorphic event.

Conversely, the satellite M2 monazites of sample 2 show ages that clearly link them to the Cretaceous subduction event, which was significant in this part of the Eastern Alps (Thöni and Miller 1996). Again, we have hardly means to judge if Cretaceous monazite formation mainly occurred close to the P-T peak (720°C, 14-16 kbar) or slightly earlier at lower T on the clockwise prograde path, along with garnet. The abundance of Cretaceous garnet, which acted as a sink for Y, is certainly responsible for the particularly low concentration of Y in the M2 monazite grains (Fig. 4b). The Y distribution between garnet and monazite (Pyle et al. 2001) could eventually permit more information on the crystallization interval of the monazite. However, such data are presently not at hand. The fact that the Y contents in the Cretaceous monazite are constantly low,

may be taken as a qualitative argument in favour of a mainly post-garnet monazite growth, which would, in turn, imply monazite formation close to the temperature peak.

For sample 3 (meta-granitoid, Ötztal Crystalline Unit), two moderately precise age dates of 478±11 Ma and 343±15 Ma could be derived for the M1 and M2 monazite grains. The older M1 monazite generation is most probably magmatic in that rock. This interpretation is independently supported by the high Y_2O_3 contents in some of these M1 monazite grains (Fig. 5c), which indicate crystallization temperatures of around 700 °C or higher (Heinrich et al. 1997, Pyle et al. 2002).

The age of 343±15 Ma, determined for the satellite M2 monazites, falls during the period of the Variscan orogeny. The Variscan event has also been recorded by other methods in this area, such as Sm-Nd garnet dating (Thöni 2003). Satellite M2 monazite formation in sample 3 is thus significantly older than in samples 1 and 2. Notably, the satellite M2 monazites in sample 3 show a marginal reaction to fluorapatite and allanite, which is most likely the result of greenschist-facies Alpine metamorphism during the Cretaceous. Thus, in the confined space of a few dozen microns, a microstructural record of ~ 500 Ma and three orogenies are recorded.

Mineral reactions

The monazite microstructures, described above, are essentially based on two mineral reactions. These include the marginal or complete breakdown of a (large) pre-existing monazite grain to fluorapatite + allanite (reaction A) and the back-reaction of fluorapatite + allanite to monazite (reaction B).

The corona-forming reaction A has been considered in a number of previous studies (Broska and Siman 1998, Finger et al. 1998, Grapes et al. 2005, Majka and Budzyn 2006, Upadhyay and Pruseth 2012), based on cases where no satellite M2 monazites formed. Because reaction A

prepares the ground for potential later satellite M2 monazite formation in the corona, it is worthwhile to recall the main reaction mechanisms. Reaction A involves a replacement of M1 monazite by fluorapatite due to the addition of external Ca + F (see e.g. Fig. 2a). The direct transformation of M1 monazite to fluorapatite is a favourable reaction mechanism, because the PO_4 tetrahedra of the monazite need not to be destroyed and can be taken as building blocks directly into the fluorapatite structure. The LREEs liberated from M1 monazite breakdown, migrate a few microns through the fluorapatite ring and precipitate together with externally derived Al, Si, Fe, and Ca ions as an allanite corona. The source of the external elements has been variably assessed in the literature. Minerals like carbonate, biotite, or epidote are possible reactants (Broska and Siman 1998, Wing et al. 2003, Grapes et al. 2005, Budzyn et al. 2011). The fact that a distal rim of epidote commonly surrounds the allanite (Fig. 2a) may indicate a simultaneous epidote-producing reaction. Retrograde epidote formation, at the expense of plagioclase is a widely observed process in the temperature range in which these fluorapatite-allanite coronas commonly form (350-550 °C). Thus, for reaction A we may be facing a tandem reaction in which a certain amount of newly formed epidote, from an external source (e.g., plagioclase), reacts with M1 monazite to form fluorapatite and allanite. Epidote will continue to overgrow the allanite in an epitaxial relationship.

Microstructural observations suggest that satellite M2 monazite formation through reaction B occurs preferentially at the contact between the fluorapatite and the allanite ring or within the allanite zone (Figs. 2a and 2c). In sample 2 (Fig. 2b), the allanite has been widely consumed, but the geometry of the satellite M2 monazites implies that a fluorapatite-allanite corona, comparable to Fig. 2a, was present at some earlier stage. Interestingly, M2 monazite is rarely seen enclosed in the fluorapatite zone, so that there is commonly some space between the core M1 monazite and the satellite M2 monazite grains. Hence, these older and younger monazite grains can and will

often occur in proximity to each other but without growing together to form composite polygenetic grains. Minute inclusions of Th-Si rich minerals (thorite or huttonite), which are present in the fluorapatite zone, are probably products of M1 monazite resorption via reaction A, because they also occur in fluorapatite-allanite coronas that lack satellite monazite grains (see Finger et al. 1998).

In the case of sample 2 (Fig. 2a), appreciable amounts of mica and chlorite are found in the corona. These minerals may have taken up a portion of the Si, Al and Fe liberated from allanite-apatite breakdown. However, as evidenced by K_2O migration, the allanite-fluorapatite corona is by no means a closed system, and some element exchange with the rock matrix inevitably takes place. As can be seen in sample 2 (Fig. 2b), the apatite-allanite corona tends to disappear at higher metamorphic temperatures and be replaced by micas, which fill in the space between the M2 monazite grains.

Textural modifications

In sample 1 (Fig. 2a), reactions A and B are both frozen approximately half way to completion and a large remnant M1 monazite core is always preserved. In sample 3 the situation is different in that reaction A has completely consumed the older core M1 monazite in several cases, and fluorapatite dominates the central parts of the structure (Fig. 5a). Another modification, observed in sample 3, is that the satellite M2 monazites themselves became unstable during a later geological event and spawned their own smaller metamorphic apatite-epidote coronas (Fig. 5b).

In sample 2, we observe that reaction A is mostly halfway complete, i.e. M1 monazite grains are almost always present, while reaction B is nearly complete (Fig. 2b). The allanite-epidote ring has become consumed to a large extent and replaced by muscovite, some biotite, and some kyanite (Fig. 2b). The remnant fluorapatite ring has recrystallized to individual euhedral grains

with a different crystallographic orientation. In addition, we find small rims of new metamorphic monazite fringing the remnant M1 monazite cores (Fig. 2b). These younger overgrowth shells correspond chemically to the M2 satellite grains. They could develop because the "shielding" apatite ring was strongly thinned out here through reaction B, which permitted the new monazite to amalgamate with the core monazite. Through this process, composite age, zoned monazite grains could form.

Another notable parameter is the size of the satellite M2 monazites. In sample 1 (Fig. 2a), the satellite M2 monazite grains are numerous but always anhedral and tiny, most probably because the metamorphic temperatures during M2 monazite formation remained rather low (400 – 450 °C). The fluorapatite-allanite corona is consumed only to a moderate extent. In sample 2, the satellite M2 monazites on average have become somewhat larger in size (up to 20 μm), but they are less numerous possibly due to localized Ostwald ripening. The largest satellite M2 monazites are observed in sample 3 (up to 30 μm), despite the fact that metamorphic peak temperatures were probably lower than in sample 2 (650 vs. 720 °C), though the duration of the metamorphic event might have been longer.

There is sporadic evidence in sample 2 that, in favourable cases, both reactions A and B can go to completion. Concentric rings of small M2 monazite grains are the result (Fig. 5 c). Tectonic strain will increasingly deform these M2 monazite rings such that chains and irregular clusters of monazites will form instead (Fig. 5d). The geometry of M2 clusters (rings or chains) can thus potentially give information on the degree of rock deformation. Naturally, there is always the chance that a piece of a relict M1 monazite might be hidden in these M2 monazite clusters. Subsequently in any in-situ geochronological study, it would be worthwhile to target as many grains as possible in a monazite cluster.

404 **Mechanisms of monazite formation in regional metamorphic terrains**

405 Our three case studies provided no analytical evidence for a major resetting of the Th-U-Pb
406 system in the M1 monazite. Only in sample 2, where the metamorphic temperatures were highest
407 (720 °C during the Alpine event), is a thin overgrowth visible around the M1 monazite grains.
408 Apart from that, no younger domains (or domains with Pb loss) could be identified within the M1
409 monazite. Therefore, we would like to make the tentative conclusion here that monazite
410 recrystallization (i.e., *in situ* replacement of older monazite by younger monazite) is not a very
411 common process in greenschist-facies and lower to middle amphibolite-facies regional
412 metamorphic terrains, even though special fluid-rich conditions can occasionally provoke
413 monazite recrystallization in this temperature range (Rasmussen et al. 2007, Williams et al. 2011,
414 Didier et al. 2013). The situation probably changes significantly at higher, i.e., upper
415 amphibolite- to granulite-facies metamorphic temperatures. Here, monazite-recrystallization
416 through coupled dissolution-reprecipitation appears to become a much more dominant process
417 (Harlov et al. 2011), which explains why little if any inherited monazite can survive in such high-
418 grade rocks (Parrish 1990, Rubatto et al. 2001).

419 Our study nicely confirms earlier observations that metamorphic monazite can form by reaction
420 from fluorapatite and allanite (Smith and Barreiro 1990, Wing et al. 2003, Janots et al. 2007,
421 2008, Spear 2010) and, indeed, provides for the first time unequivocal microstructural evidence
422 for that process. However, it also implies that, in the absence of fluids capable of transporting
423 LREEs and P, metamorphic monazite will commonly remain small, forming only in sites where
424 apatite and allanite have been in contact. On the other hand, several geochronological studies of
425 medium grade metapelites have decribed monazite grains much larger than 30 μm (Parrish 1990,
426 Smith and Barreiro 1990, Foster et al. 2002). This leaves room for speculations that fairly often in
427 metamorphic systems, fluid-aided transport of the LREEs and P might play a role. When, where,

and how often such fluid-aided processes contribute to metamorphic monazite growth, and if they can transport REEs and P only locally on the mm scale or over larger distances, is debatable. The present study gives no real answers to these questions, because it refers to selected samples where the REEs may have been particularly immobile. A more detailed investigation over a broader range of samples would first be needed to begin to answer these questions. There is firm evidence that in certain cases LREE- and P-bearing fluids are present in metamorphic rocks, even at low to medium temperature conditions, and that monazite can easily precipitate from these fluids (Didier et al. 2013, Gnos et al. 2015).

IMPLICATIONS FOR PETROLOGY AND GEOCHRONOLOGY

Our three case studies underline the importance of a prograde allanite-to-monazite transition in metamorphic terrains as described in petrographic observations (Bingen et al. 1996; Wing et al. 2003; Janots et al. 2008) and charted out in thermodynamic calculations (Janots et al. 2007; Spear 2010). Our results are broadly consistent with the models of Spear (2010), which describe the allanite-monazite transition as a function of P, T, X_{Ca} and X_{Al}. Taking sample 1, for instance, which is a low-Ca metapelite, the model of Spear (2010) would predict "monazite-in" at ~400 °C (at 5 kbar), which agrees well with the P-T conditions for the sampling site (400-450 °C during the Alpine event). We can thus confirm that in low-Ca metapelites monazite growth starts in the upper greenschist facies, in paragenesis with chlorite.

In samples 2 and 3, M2 monazite formation was accompanied by a temperature rise to 720° and 650 °C, respectively. The model of Spear (2010) would predict "monazite-in" at ~ 550 °C for both rocks. Hence, temperatures should have been deep within the monazite stability field in case of sample 2 (720 °C), which explains why reaction B is nearly complete here.

Nevertheless, an additional petrological aspect should not be overlooked in this context. Whether or not new monazite forms in a polymetamorphic rock will not only depend on the whole rock geochemistry and the peak metamorphic conditions. It will also depend on the precursor reaction A, which converts the pre-existing M1 monazite to fluorapatite and allanite, thereby creating the reactants for the M2 monazite producing reaction B. When no retrograde allanite is produced in a monazite bearing rock, a younger generation of metamorphic M2 monazite cannot form by reaction B. New monazite could in this case only form from P- and LREE-bearing fluids or by recrystallization.

From a geological perspective, this means that a polymetamorphic, monazite-bearing rock will become the most fertile for new monazite growth when it passes a phase of strong retrogression between the *P*-*T* peaks. In the case of orogenic events, that are temporally far apart, such low-T periods will commonly be interspaced between the metamorphic peaks. Nevertheless, there can be still two reasons why allanite fails to form during these low-T periods. One possible reason is that the whole rock chemistry may not have permitted its growth, which could be true in the case of very Ca-poor rocks (for instance, quartzites). Such Ca-poor rocks may thus be predestined to conserve older monazite. In the second scenario, lack of allanite formation could simply be due to sluggish reaction kinetics. Formation of retrograde REE carbonates at the expense of the original monazite may stimulate a later metamorphic growth of monazite as well, although monazite formation from an REE carbonate precursor has, to our knowledge, until now not been reported in the literature.

The main conclusion from this survey is that in most polymetamorphic rock units there will be certain lithologies where newly formed monazite will preferentially appear and others that will tend to preserve inherited monazite. The challenge here is for geochronologists to apply both the proper sampling strategies and a careful petrographic/mineralogical examination of each sample.

475 Knowing the reaction processes that create and destroy monazite in polymetamorphic rocks
476 should be one major step in this direction.
477

478 **ACKNOWLEDGEMENTS**

479 Michael Waitzinger is thanked for analytical assistance on the SEM. Financial support through
480 the Austrian Science Fund (FWF project P 22480 to F. Finger) and the Deutsche
481 Forschungsgemeinschaft (DFG project Schu 676/13-1, 13-2 to B. Schulz) are gratefully
482 acknowledged. Thorough reviews by I. Broska, P. Lanari and J.M. Montel helped to improve the
483 manuscript.
484

485 **REFERENCES**

486 Bankhammer, A. (2004) Untersuchungen zur Petrogenese der altkristallinen Gesteine des
487 Zwölferzugs am Nordrand des Tauernfensters (Land Salzburg). Diploma thesis, pp 112.
488 Bingen, B., Demaiffe, D., and Hertogen, J. (1996) Redistribution of rare earth elements, thorium,
489 and uranium over accessory minerals in the course of amphibolite to granulite facies
490 metamorphism; the role of apatite and monazite in orthogneisses from south western Norway.
491 Geochimica et Cosmochimica Acta, 60, 1341-1354.
492 Broska, I., and Siman, P. (1998) The breakdown of monazite in the West-Carpathian Veporic
493 orthogneisses and Tatric granites. Geologica Carpathica, 49, 161-167.
494 Budzyn, B., Harlov, D.E., Williams, M.L., and Jercinovic, M.J. (2011) Experimental
495 determination of stability relations between monazite, fluorapatite, allanite, and REE-epidote
496 as a function of pressure, temperature, and fluid composition. American Mineralogist, 96,
497 1547-1567.

498 Dachs, E., Frasl, G., and Hoinkes, G. (1991) Mineralogisch-Petrologische Exkursion ins
499 Penninikum des Tauernfensters (Großglockner Hochalpenstraße/Südliches Großvenediger
500 Gebiet) und in das Ötztalkristallin (Timmelsjoch/Schneebergerzug). European Journal of
501 Mineralogy, 3, 79-110.
502 Didier, A., Bosse, V., Boulvais, P., Bouloton, J., Paquette, J.L., Montel, J.M., and Devidal, J.L.
503 (2013) Disturbance versus preservation of U-Th-Pb ages in monazite during fluid-rock
504 interaction: textural, chemical and isotopic in situ study in microgranites (Velay Dome,
505 France). Contributions to Mineralogy and Petrology, 165, 1051-1072.
506 Didier, A., Bosse, V., Cherneva, Z., Gautier, P., Georgieva, M., Paquette, J.L., and Gerdjikov, I.
507 (2014) Syn-deformation fluid-assisted growth of monazite during renewed high-grade
508 metamorphism in metapelites of the Central Rhodope (Bulgaria, Greece). Chemical Geology,
509 381, 206-222.
510 Finger, F., Broska, I., Roberts, M.P., and Schermaier, A. (1998) Replacement of primary
511 monazite by apatite-allanite-epidote coronas in an amphibolite-facies granite gneiss from the
512 eastern Alps. American Mineralogist, 83, 248-258.
513 Foster, G., Gibson, H.D., Parrish, R., Horstwood, M., Fraser, J., and Tindle, A. (2002) Textural,
514 chemical and isotopic insights into the nature and behaviour of metamorphic monazite.
515 Chemical Geology, 191, 183-207.
516 Frank, W., Miller, C., and Pestal, G. (1987) Geologische Karte der Republik Österreich 1:50000,
517 Blatt 152 Matrei in Osttirol. Geologische Bundesanstalt Wien.
518 Gasser, D., Bruand, E., Rubatto, D., and Stüwe, K. (2012) The behaviour of monazite from
519 greenschist facies phyllites to anatectic gneisses: An example from the Chugach Metamorphic
520 Complex, southern Alaska. Lithos, 134-135, 108–122.

Gieré, R., and Sorensen, S.S. (2004) Allanite and other REE-rich epidote group minerals. Reviews in Mineralogy, 56, 431–494.

Gnos, E., Janots, E., Berger, A., Whitehouse, M., Walter, F., Pettke, T., and Bergemann, C. (2015) Age of cleft monazites in the eastern Tauern Window: constraints on crystallization conditions of hydrothermal monazite. Swiss Journal of Geoscience, DOI 10.1007/s00015-015-0178-z.

Goswami-Banerjee, S., Robyr, M. (2015) Pressure and temperature conditions for crystallization of metamorphic allanite and monazite in metapelites: a case study from the Miyar Valley (high Himalayan Crystalline of Zanskar, NW India). Journal of metamorphic Geology, 33, 535-556.

Grapes, R., Bucher, K., and Hoskin, P.W.O. (2005) Monazite-epidote reaction in amphibolite grade blackwall rocks. European Journal of Mineralogy, 17, 553-566.

Harlov, D.E., Wirth, R., and Hetherington, C.J. (2011) Fluid-mediated partial alteration of monazite: the role of coupled dissolution-reprecipitation in element redistribution and mass transfer. Contributions to Mineralogy and Petrology, 162, 329-348.

Heinrich, W., Andrehs, G., and Franz, G. (1997) Monazite-xenotime miscibility gap thermometry. I. An empirical calibration. Journal of Metamorphic Geology, 15, 3-16.

Hirtopanu, P., Jakab, G., Andersen, C.J., and Fairhurst, J.R. (2013) Thorite, thorogummite and xenotime-(Y) occurrence in Ditrau alkaline intrusive massif, East Carpathians, Romania. Proceedings of the Romanian Academy, Series B: Chemistry, Life Sciences and Geoscience, 15(2), 111–132.

Hoinkes, G., Thöni, M., Lichem, C., Bernhard, F., Kaindl, R., Schweigl, J., Tropper, P., and Cosca, M. (1997) Metagranitoids and associated metasediments as indicators for the pre-Alpine magmatic and metamorphic evolution of the western Ötztal Basement (Kaunertal, Tirol). Schweizer Mineralogisch Petrographische Mitteilungen, 77, 299-314.

545 Janots, E., Brunet, F., Goffe, B., Poinssot, C., Burchard, M., and Cemic, L. (2007)
546 Thermochemistry of monazite-(La) and dissakisite (La): implications for monazite and allanite
547 stability inmetapelites. Contributions to Mineralogy and Petrology, 154, 1-14.
548 Janots, E., Engi, M., Berger, A., Allaz, J., Schwarzc, J.O., and Spandler, C. (2008) Prograde
549 metamorphic sequence of REE minerals in pelitic rocks of the Central Alps: implications for
550 allanite–monazite–xenotime phaserelations from 250 to 610 °C. Journal of Metamorphic
551 Geology, 26, 509-526.
552 Jercinovic, M.J., and Williams, M.L. (2005) Analytical perils (and progress) in electron
553 microprobe trace element analysis applied to geochronology: background acquisition,
554 interferences, and beam irradiation effects. American Mineralogist, 90, 526–546.
555 Krenn, E., and Finger, F. (2006) Satellite monazites: A peculiar microstructural feature in
556 polymetamorphic basement rocks of the Alps and its origin. Geophysical Research Abstracts
557 8, 07578, EGU Vienna.
558 Krenn E, Ustaszewski K, Finger F (2008) Detrital and newly formed metamorphic monazite in
559 amphibolite-facies metapelites from the Motajica Massif, Bosnia. Chemical Geology 254:
560 164-174
561 Lee, D.E., and Bastron, H. (1967) Fractionation of rare-earth elements in allanite and monazite as
562 related to geology of the Mt. Wheeler mine area, Nevada. Geochimica et Cosmochimica Acta,
563 31, 339-356.
564 Lee, D.E., and Dodge, F.C.W. (1964) Accessory minerals in some granitic rocks in California
565 and Nevada as a function of Calcium content. American Mineralogist ,49, 1660-1669.
566 Majka, J., and Budzyn, B. (2006) Monazite breakdown in metapelites from Wedel Jarlsberg
567 Land, Svalbard - Preliminary results. Mineralogia Polonica, 37, 61-69.

568 Montel, J.M., Foret, S., Veschambre, M., Nicollet, Ch., and Provost, A. (1996) Electron
569 microprobe dating of monazite. Chemical Geology, 131, 37-53.
570 Ondrejka, M., Uher, P., Putis, M., Broska, I., Bacik P., Konecny, P. (2012) Two-stage breakdown
571 of monazite by post-magmatic and metamorphic fluids: An example from the Veporic
572 orthogneiss, Western Carpathians, Slovakia. Lithos, 142-143, 245-255.
573 Parrish, R.R. (1990) U-Pb dating of monazite and its application to geological problems.
574 Canadien Journal of Earth Science, 27, 1431-1450.
575 Pyle, J.M., Spear, F.S., Rudnick, R.L., and McDonough, W.F. (2001) Monazite–xenotime–garnet
576 equilibrium in metapelites and a new monazite–garnet thermometer. Journal of Petrology, 42,
577 2083–2107.
578 Pyle, J.M., Spear, F.S., and Wark, D.A. (2002) Elektron microprobe analysis of REE in apatite,
579 monazite and xenotime: protocols and pitfalls. Reviews in Mineralogy, 48, 338-362.
580 Rasmussen, B., Fletcher, I.R., and Muhling, J.R. (2007) In situ U–Pb dating and element
581 mapping of three generations of monazite: unravelling cryP-Tic tectonothermal events in low-
582 grade terranes. Geochimica et Cosmochimica Acta, 71, 670–690.
583 Rode, S., Rösel, D., and Schulz, B. (2012) Constraints on the Variscan P-T evolution by EMP
584 Th-U-Pb monazite dating in the polymetamorphic Austroalpine Oetztal-Stubai basement
585 (Eastern Alps). Zeitschrift der Deutschen Gesellschaft für Geowissenschaften, 163, 43-67.
586 Romer, R.L., and Siegesmund, S. (2003) Why allanite may swindle about its true age.
587 Contributions to Mineralogy and Petrology, 146, 297-307.
588 Rubatto, D., Williams, I.S., and Buick, I.S. (2001) Zircon and monazite response to prograde
589 metamorphismin the Reynolds Range, central Australia. Contributions to Mineralogy and
590 Petrology, 140, 458–468.

591 Schindlmayr, A. (1999) Granitoids and Plutonic Evolution of the Ötztal-Stubai Massif - A Key
592 for Understanding the Early Palaeozoic History of the Austroalpine Crystalline Basement in
593 the Western Eastern Alps. PhD thesis Salzburg University, 288 p.
594 Schmid, S.M., Fügenschuh, B., Kissling, E., and Schuster, R. (2004) Tectonic map and overall
595 architecture of the Alpine orogen. Eclogae Geologicae Helvetiae, 97, 93-117.
596 Schulz, B. (2013) Two metamorphic cycles recorded by garnet and monazite in micaschists from
597 the Saualpe Eclogite Zone (Eastern Alps). Schriftenreihe der Deutschen Gesellschaft für
598 Geowissenschaften, 82, 98.
599 Schulz, B., and Schüssler, U. (2013) Electron-microprobe Th-U-Pb monazite dating in Early-
600 Paleozoic high-grade gneisses as a completion of U-Pb isotopic ages (Wilson Terrane,
601 Antarctica). Lithos, 175–176, 178–192.
602 Schuster, R., and Stüwe, K. (2008) Permian metamorphic event in the Alps. Geology, 36, 603-
603 606.
604 Shaw, D.M. (1956) Geochemistry of pelitic rocks. Part III: major elements and general
605 geochemistry. Geological Society of America Bulletin, 67, 919–934.
606
607 Smith, H.A., and Barreiro, B. (1990) Monazite U-Pb dating of staurolite grade metamorphism in
608 pelitic schists. Contributions to Mineralogy and Petrology, 105, 602-615.
609 Spear, F.S., and Pyle, J.M. (2002) Phosphates in metamorphic rocks. Reviews in Mineralogy, 48,
610 293–335.
611 Spear, F.S. (2010) Monazite–allanite phase relations in metapelites. Chemical Geology, 279, 55-
612 62.

613 Suzuki, K., Adachi, M., and Tanaka, T. (1991) Middle Precambrian provenance of Jurassic
614 sandstone in the Mino Terrane, central Japan: Th-U-total Pb evidence from an electron
615 microprobe monazite study. Sedimentary Geology, 75, 141-147.
616 Thöni, M. (2003) Sm-Nd isotope systematics in garnet from different lithologies (Eastern Alps):
617 age results, and an evaluation of potential problems for garnet Sm-Nd chronometry. Chemical
618 Geology, 194, 353-379.
619 Thöni, M., and Miller, Ch. (1996) Garnet Sm-Nd data from the Saualpe and the Koralpe (Eastern
620 Alps, Austria): chronological and P-T constraints on the thermal and tectonic history. Jounal
621 of Metamorphic Geology, 14, 453-466.
622 Tropper, P., and Recheis, A. (2003) Garnet zoning as a window into the metamorphic evolution
623 of a crystalline complex: the northern and central Austroalpine Ötztal-Complex as a
624 polymorphic example. Mitteilungen der Österreichischen Geologischen Gesellschaft 94, 27-
625 53.
626 Upadhyay, D., and Pruseth, K.L. (2012) Fluid-induced dissolution breakdown of monazite from
627 Tso Morari complex, NW Himalayas: evidence for immobility of trace elements.
628 Contributions to Mineralogy and Petrology, 164, 303-316.
629 Von Quadt, A. (1992) U-Pb zircon and Sm-Nd geochronology of mafic and ultramafic rocks
630 from the central part of the Tauern Window (eastern Alps). Contributions to Mineralogy and
631 Petrology, 110, 57-67.
632 Weissenbach, N., and Pistotnik, J. (2000) Geologische Karte 1 : 50 000 Blatt 187 Bad Sankt
633 Leonhard im Lavanttal. Geologische Bundesanstalt Wien
634 Wing, B., Ferry, J.M., and Harrison, T.M. (2003) Prograde destruction and formation of monazite
635 and allanite during contact and regional metamorphism of pelites: petrology and
636 geochronology. Contribution to Mineralogy and Petrology, 145, 228-250.

637 Williams, M.L., Jercinovic, M.J., Harlov, D.E., Budzyn, B., and Hetherington, C.J. (2011)
638 Resetting monazite ages during fluid-related alteration. Chemical Geology, 283, 218-225.
639
640

641 **Figures and Tables**

642

643 Fig. 1: Geological sketch map of the Eastern Alps after Schmidt et al. (2004) showing the sample
644 locations for this study.

645

646 Fig. 2: Representative examples of satellite monazite grains in samples 1, 2 and 3.

647

648 Fig. 3: Th-U-Pb monazite dating results on M1 and M2 grains shown in isochron diagrams after
649 Suzuki et al. (1991). Th* and Pb values are wt. %. Scale on right side shows the major orogenic
650 events in the Eastern Alps (VO: Variscan Orogeny, PR: Permian Rifting, AO: Alpine orogeny)

651

652 Fig. 4: Y_2O_3 vs. UO_2 diagrams showing the compositions of M1 and M2 monazite in samples 1,
653 2 and 3. Values in wt. %.

654

655 Fig. 5: Examples of modified reaction textures. a: the core monazite is completely replaced by
656 fluorapatite (sample 3); b: the satellite monazites are marginally replaced by a fluorapatite-
657 allanite ring due to a renewed low-T overprint (sample 3; cf. Fig. 2c); c, d: clusters of small
658 newly formed monazite grains featuring an advance stage of destruction of former fluorapatite-
659 allanite coronas (sample 2).

660

661

662 Table 1: Selected electron microprobe analyses of M1 and M2 monazite grains from samples 1, 2
663 and 3 with Th-U-Pb ages and errors (2 σ). Formula units calculated on the basis of 4 oxygens. * =
664 rim zone

This is a preprint, the final version is subject to change, of the American Mineralogist (MSA)
Cite as Authors (Year) Title. American Mineralogist, in press.
(DOI will not work until issue is live.) DOI: http://dx.doi.org/10.2138/am-2016-5477

	Sample 1				Sample 2					Sample 3			
	M1	M1	M2	M2	M1	M1	M1*	M2	M2	M1	M1	M2	M2
SiO_2	0.26	0.45	< d.l.	< d.l.	0.18	0.34	0.55	0.33	0.49	0.13	0.16	0.10	0.25
P_2O_5	29.07	28.54	29.70	29.91	30.31	30.19	29.64	29.77	29.57	29.88	29.94	29.62	29.24
CaO	0.99	1.07	0.88	0.88	0.97	1.20	1.26	0.87	0.93	1.20	1.22	1.24	1.27
Y_2O_3	0.03	< d.l.	1.02	1.13	1.89	1.78	0.08	0.16	0.18	3.77	3.63	1.45	1.72
La_2O_3	13.11	13.57	11.50	13.97	14.01	13.60	18.03	15.76	15.02	11.34	11.71	11.83	13.57
Ce_2O_3	30.04	30.78	28.58	31.63	28.08	26.91	29.25	30.08	29.41	26.43	26.83	29.10	29.45
Pr_2O_3	3.66	3.56	3.57	3.52	3.04	2.80	2.67	3.00	3.06	3.75	3.65	3.17	3.31
Nd_2O_3	12.75	13.03	13.10	12.39	12.27	12.27	9.49	11.89	11.75	11.96	12.05	11.63	11.05
Sm_2O_3	2.42	2.36	2.57	2.20	2.28	2.29	1.04	1.51	1.61	2.39	2.35	2.42	1.99
Gd_2O_3	1.02	0.84	1.15	0.93	1.56	1.61	0.49	0.87	0.97	1.88	1.94	1.77	1.48
Dy_2O_3	< d.l.	< d.l.	0.49	0.21	< d.l.	< d.l.	< d.l.	< d.l.	< d.l.	0.78	0.73	0.64	0.51
Er_2O_3	< d.l.	< d.l.	0.16	0.07	< d.l.	< d.l.	< d.l.	< d.l.	< d.l.	0.26	0.24	0.21	0.17
Yb_2O_3	< d.l.	< d.l.	< d.l.	< d.l.	< d.l.	< d.l.	< d.l.	< d.l.	< d.l.	0.09	0.08	0.07	0.06
ThO_2	3.96	3.24	5.03	1.90	4.15	5.82	7.10	4.22	5.30	4.93	5.12	5.52	4.79
UO_2	1.12	0.87	0.63	0.31	0.73	0.78	0.73	0.70	0.64	0.29	0.26	0.29	0.27
PbO	0.11	0.08	0.01	0.01	0.09	0.12	0.05	0.03	0.04	0.12	0.12	0.13	0.08
Total	98.53	98.41	98.38	99.04	99.55	99.70	100.38	99.20	98.98	99.19	100.05	99.19	99.21
Si	0.010	0.018	0.000	0.000	0.007	0.013	0.021	0.013	0.019	0.005	0.006	0.004	0.010
P	0.984	0.970	1.001	0.994	0.995	0.991	0.977	0.988	0.984	0.990	0.987	0.992	0.979
Ca	0.042	0.046	0.038	0.037	0.040	0.050	0.053	0.037	0.039	0.050	0.051	0.053	0.054
Y	0.001	0.000	0.022	0.024	0.039	0.037	0.002	0.003	0.004	0.079	0.075	0.030	0.036
La	0.193	0.201	0.169	0.202	0.200	0.194	0.259	0.228	0.218	0.164	0.168	0.173	0.198
Ce	0.440	0.453	0.417	0.455	0.398	0.382	0.417	0.431	0.423	0.379	0.383	0.422	0.427
Pr	0.053	0.052	0.052	0.050	0.043	0.040	0.038	0.043	0.044	0.053	0.052	0.046	0.048
Nd	0.182	0.187	0.186	0.174	0.170	0.170	0.132	0.166	0.165	0.167	0.168	0.164	0.156
Sm	0.033	0.033	0.035	0.030	0.030	0.031	0.014	0.020	0.022	0.032	0.032	0.033	0.027
Gd	0.014	0.011	0.015	0.012	0.022	0.022	0.007	0.012	0.014	0.024	0.025	0.023	0.019

table1

Dy	0.000	0.000	0.006	0.003	0.000	0.000	0.000	0.000	0.000	0.010	0.009	0.008	0.006
Er	0.000	0.000	0.002	0.001	0.000	0.000	0.000	0.000	0.000	0.003	0.003	0.003	0.002
Yb	0.000	0.000	0.000	0.000	0.000	0.000	0.000	0.000	0.000	0.001	0.001	0.001	0.001
Th	0.036	0.030	0.046	0.017	0.037	0.051	0.063	0.038	0.047	0.044	0.045	0.050	0.043
U	0.010	0.008	0.006	0.003	0.006	0.007	0.006	0.006	0.006	0.003	0.002	0.003	0.002
Pb	0.001	0.001	0.000	0.000	0.001	0.001	0.001	0.000	0.000	0.001	0.001	0.001	0.001
Tetr.	0.995	0.989	1.001	0.994	1.002	1.004	1.002	1.001	1.003	0.995	0.993	0.996	0.989
A[9]	1.006	1.021	0.993	1.007	0.987	0.984	0.987	0.985	0.982	1.011	1.015	1.009	1.021
Age	356	326	61	49	253	276	91	77	96	496	470	366	317
Error	54	67	58	142	79	61	54	79	70	69	68	60	72

table1

This is a preprint, the final version is subject to change, of the American Mineralogist (MSA)
Cite as Authors (Year) Title. American Mineralogist, in press.
(DOI will not work until issue is live.) DOI: http://dx.doi.org/10.2138/am-2016-5477

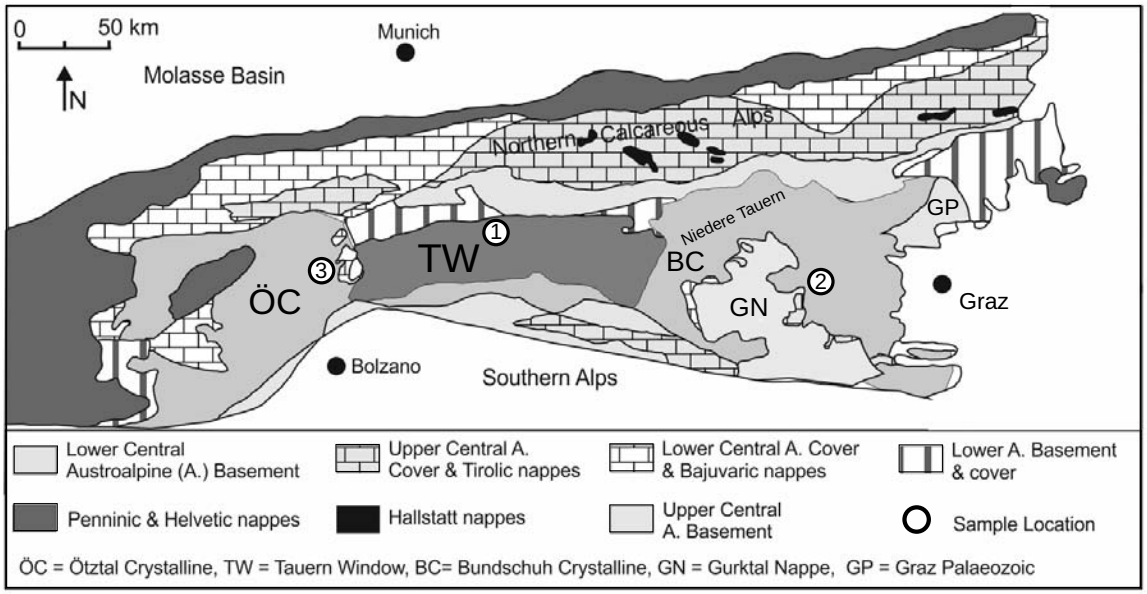

Figure 1

This is a preprint, the final version is subject to change, of the American Mineralogist (MSA)
Cite as Authors (Year) Title. American Mineralogist, in press.
(DOI will not work until issue is live.) DOI: http://dx.doi.org/10.2138/am-2016-5477

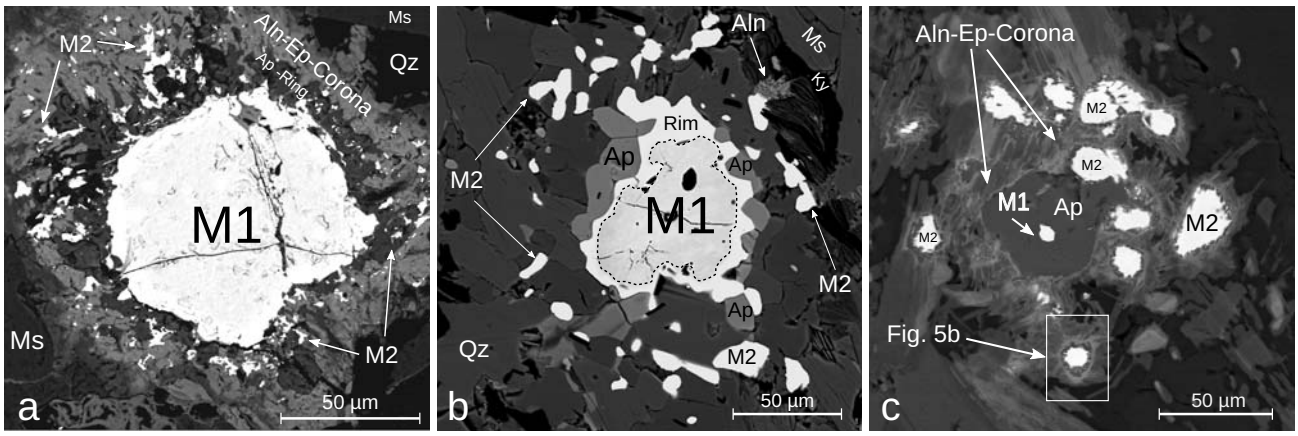

Figure 2a,b,c

This is a preprint, the final version is subject to change, of the American Mineralogist (MSA)
Cite as Authors (Year) Title. American Mineralogist, in press.
(DOI will not work until issue is live.) DOI: http://dx.doi.org/10.2138/am-2016-5477

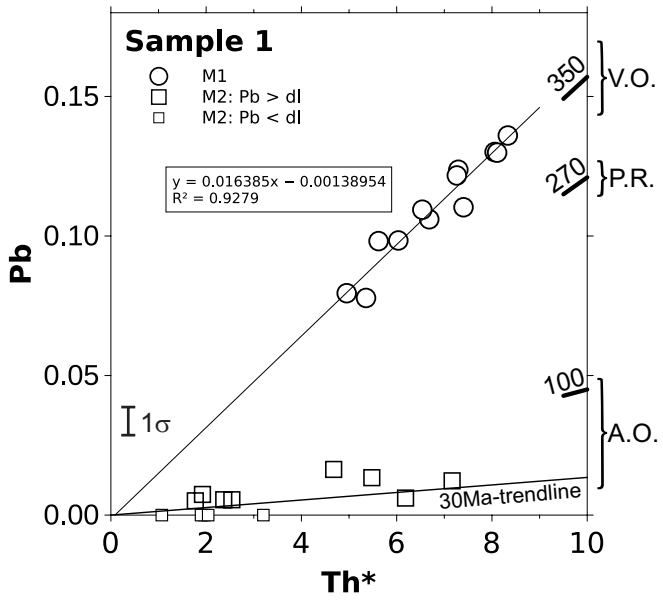

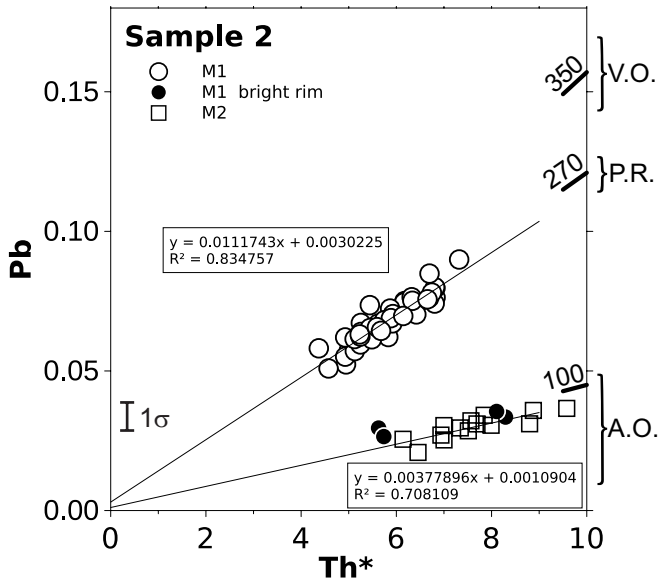

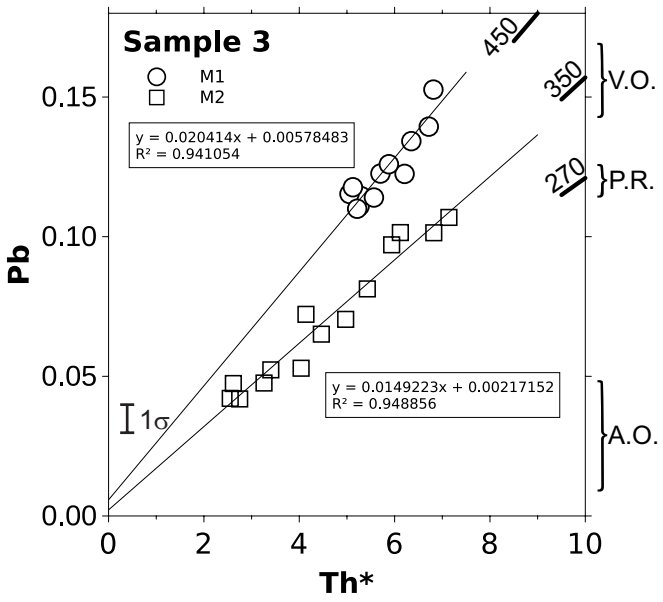

This is a preprint, the final version is subject to change, of the American Mineralogist (MSA)
Cite as Authors (Year) Title. American Mineralogist, in press.
(DOI will not work until issue is live.) DOI: http://dx.doi.org/10.2138/am-2016-5477

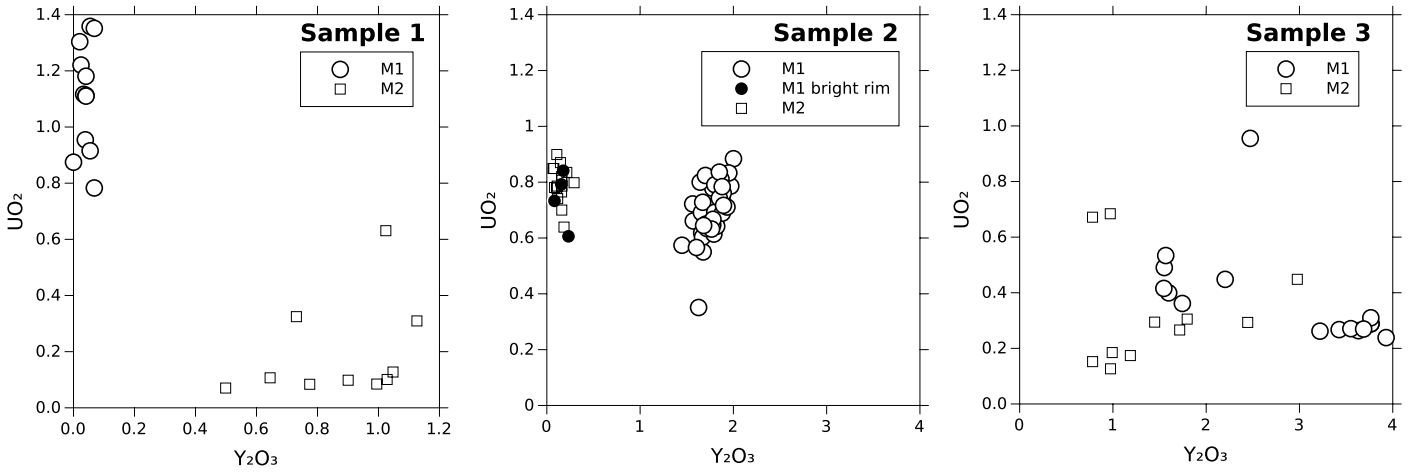

Figure 4

This is a preprint, the final version is subject to change, of the American Mineralogist (MSA)
Cite as Authors (Year) Title. American Mineralogist, in press.
(DOI will not work until issue is live.) DOI: http://dx.doi.org/10.2138/am-2016-5477

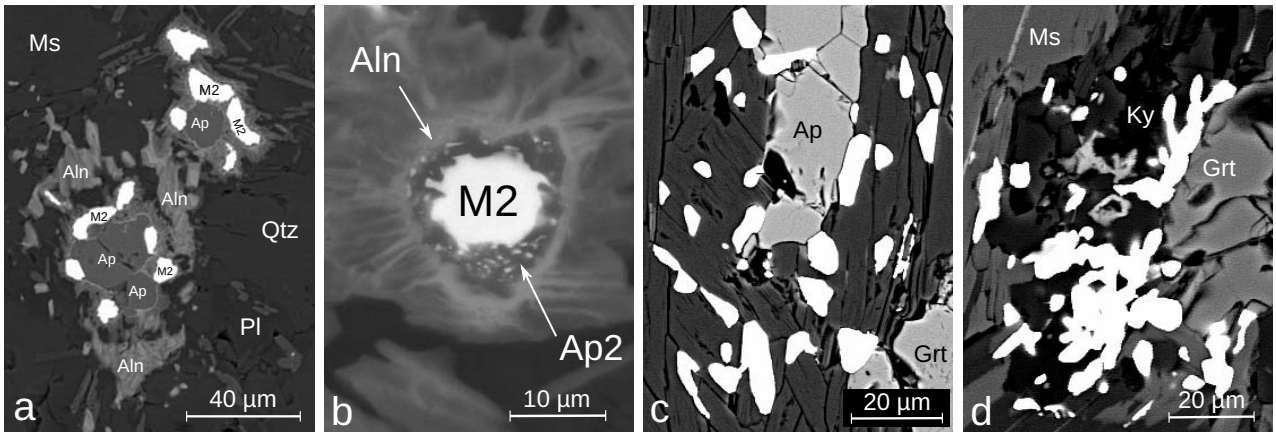

Figure 5a,b,c,d